

Phase Behavior of Short Range Square Well Model

D. L. Pagan and J. D. Gunton

Department of Physics, Lehigh University, Bethlehem, P.A. 18015

(Dated: October 30, 2018)

Abstract

Various Monte Carlo techniques are used to determine the complete phase diagrams of the square well model for the attractive ranges $\lambda = 1.15$ and $\lambda = 1.25$. The results for the latter case are in agreement with earlier Monte Carlo simulations for the fluid-fluid coexistence curve and yield new results for the liquidus-solidus lines. Our results for $\lambda = 1.15$ are new. We find that the fluid-fluid critical point is metastable for both cases, with the case $\lambda = 1.25$ being just below the threshold value for metastability. We compare our results with prior studies and with experimental results for the gamma-II crystallin.

I. INTRODUCTION

It has been known since the the work of Gast *et al.*¹, and subsequently confirmed by others^{2,3}, that the phase behavior of colloidal particles depends sensitively on the range of attraction between them. For sufficiently short range attractive interactions, the phase diagram exhibits a solid-fluid coexistence curve that is subtended by a metastable fluid-fluid coexistence curve. Such phase behavior is also typical of certain globular proteins in solution⁴. This has led scientists to model globular proteins in solution using the ideas developed in colloid science. Several models with short range attractive interactions^{6,7,8,9} have been used to calculate the phase diagrams of various proteins using computer simulation. As well, many of these models have been shown to obey a kind of van der Waal's extended states behavior¹⁰. These isotropic short-range models have also been used to characterize^{7,8} the nucleation rates for globular proteins. The simplest of these models is the square well potential, given by

$$V(r) = \begin{cases} \infty, & r < \sigma \\ -\epsilon, & \sigma \leq r < \lambda\sigma \\ 0, & r \geq \lambda\sigma. \end{cases} \quad (1)$$

The fluid-fluid coexistence curve for values of $\lambda \geq 1.25$ is known¹¹. However, to date, no direct simulation results of the complete phase diagram are available for $\lambda = 1.25$ or for smaller ranges away from the adhesive-sphere limit. This choice of $\lambda = 1.25$ for the the range of interaction is believed to be close to the threshold value below which the square well model becomes metastable. Indeed, theoretical and semi-analytical treatments confirm this hypothesis^{9,12}, although the threshold values for other short-range models is smaller. Also, the phase behavior at this value for the square well model has been compared to that of the gamma crystallin proteins¹³, mutants of which have been linked to genetic cataracts¹⁴. The square well model has also been used to determine nucleation rates at several ranges of λ to better understand protein crystallization¹⁵ and is also of interest for comparing results with theoretical approaches modelling phase behavior¹⁶, as well as for comparison with experimental studies. It is important, therefore, that these phase diagrams be accurately calculated, both at and below $\lambda = 1.25$. In this paper, we present such results using standard Monte Carlo and parallel tempering techniques.

II. COMPUTATIONAL METHODS AND DETAILS

A. Solid-fluid coexistence

Kofke¹⁷ showed that the solid-fluid coexistence curve can be obtained by solving the first-order Clausius-Clapeyron equation, given by¹⁸

$$\frac{dP}{d\beta} = -\frac{\Delta h}{\beta\Delta v} \quad (2)$$

where P is the pressure, $\beta = 1/T$ is the inverse temperature, h is the molar enthalpy, and v is the molar volume, respectively. The method, known as the Gibbs-Duhem method, requires that two isobaric-isothermal (NPT) Monte Carlo simulations be carried out in parallel so that information can be used to calculate the next state and, thus, points along the whole coexistence curve can be obtained. This method has been employed for solid-fluid coexistence for a variety of models^{6,17,19}. One *caveat* is that an initial coexistence point must first be known in order to integrate the Clausius-Clapeyron equation. To do this, the equation of state along an isotherm is obtained using NPT simulations. Once the equation of state is known, we fit the fluid-solid lines with an equation of the form

$$\beta P = \frac{\rho}{1 - a\rho} + b\left(\frac{\rho}{1 - a\rho}\right)^2 + c\left(\frac{\rho}{1 - a\rho}\right)^3 \quad (3)$$

where ρ is the number density. The solid line is fit to a 2^{nd} order polynomial equation of the form $a\rho^2 + b\rho + c$. Integrating these two equations yields the chemical potentials for the liquid and solid, as shown in equations (4) and (5), respectively.

$$\beta\mu_l = \ln\left(\frac{\rho\Lambda^2}{1 - a\rho}\right) + \frac{b/a - c/a^2 + 1}{1 - a\rho} + \frac{c/2a^2 + b\rho}{(1 - a\rho)^2} + \frac{c\rho^2}{(1 - a\rho^3)} - (b/a - c/2a^2 + 1) \quad (4)$$

$$\beta\mu_s = 2a\rho + b(\ln\rho + 1) - (a\rho^* + b\ln\rho^* - c/\rho^*) + \beta f^{ex}(\rho^*) + \ln\Lambda^2\rho^* - 1 \quad (5)$$

It should be noted that eq.(5) requires the knowledge of the free-energy at the reference density ρ^* . To calculate this, we use the Frenkel-Ladd²⁰ method of coupling a solid to harmonic springs, referred to as an Einstein lattice. The benefit of coupling the solid in this way is that the free energy of the Einstein lattice can be easily calculated analytically, allowing one to obtain the free energy of the system of interest. We consider a system that

is dependent upon a coupling parameter ξ such that the total energy of the system may be written as

$$U(\xi) = U_o + \xi U = U_o + \xi \sum_{i=1}^N (\vec{r}_i - \vec{r}_{o,i}) \quad (6)$$

where N is the number of particles, $\vec{r}_{o,i}$ the position of the lattice site to which the particle i is assigned, U_o the energy of the system of interest, and \vec{r}_i are the positions of the particles. As the coupling parameter ξ becomes large, the system becomes more strongly coupled to the lattice. For very large values the system will behave as a non-interacting Einstein lattice. To verify this behavior, the mean-squared displacements of the system for various values of ξ are computed and compared to those of a non-interacting Einstein lattice. Once this value ξ_{max} is obtained, we can calculate the free energy of the square well model at a reference density ρ^* by²¹

$$F_{SW} = F(\xi_{max}) - \int_0^{\xi_{max}} d\xi \langle U(\vec{r}^N, \xi) \rangle_{\xi}, \quad (7)$$

where the first term represents the free energy of the Einstein lattice. With the chemical potentials of both phases now known, it is straightforward to calculate a coexistence point and to subsequently perform the Gibbs-Duhem method, thereby obtaining the fluid-solid coexistence curve.

To obtain a coexistence point, NPT simulations are first performed for $N = 256$ particles in a periodic simulation cell. In one NPT simulation, on average, one volume displacement is attempted for every N attempts at displacing a particle. This is done because a volume move is computationally more expensive than a particle displacement. Equilibration runs lasted for 10 million Monte Carlo steps and production runs ran for 20 million Monte Carlo steps, a step being an attempt at either displacing a particle or changing the volume of the cell, on average. In order to compare the chemical potentials for coexistence, we must first perform simulations on a system coupled to an Einstein lattice, as described previously. We perform regular Metropolis Monte Carlo simulations on a system of $N = 256$ particles with the constraint that the center of mass of the particles remains fixed²². If a particle is given a random displacement, all particles are subsequently shifted in the opposite direction to ensure that the center of mass is constant. We update the position of the center of mass every time a trial move is accepted. Thus, the shift in the center of mass is continually

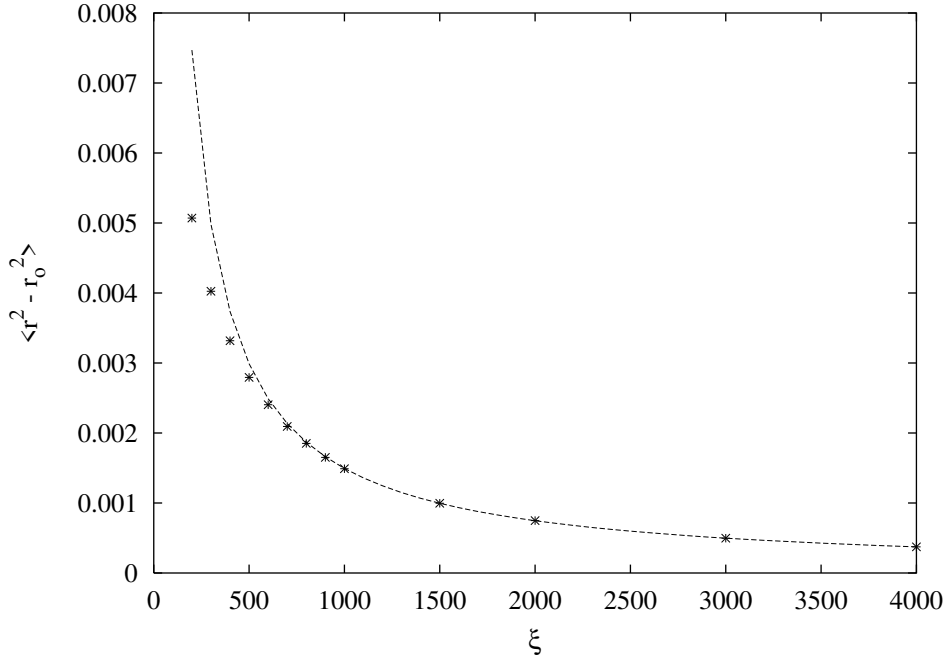


FIG. 1: Comparison of mean squared displacements for a coupled solid with that of an Einstein lattice (solid line) for the range $\lambda = 1.25$.

updated in order to properly calculate the harmonic energy contribution²². Einstein lattice simulations were equilibrated for 5 million Monte Carlo steps and were run for a total of 10 million Monte Carlo steps. These simulations are carried out at different values of the coupling parameter ξ . Fig. 1 shows our results for the mean squared displacements for $\lambda = 1.25$. We use $\xi_{max} = 4000$ at $\lambda = 1.25$ and $\xi_{max} = 3000$ at $\lambda = 1.15$ for the square well systems, respectively. The integral in eq. (5) is evaluated using a 10-point Gaussian quadrature²³ to obtain the free energy of the square well system. Once this free energy is obtained, the chemical potentials are plotted versus pressure to obtain a coexistence point, given by the point at which the two curves intersect.

The Gibbs-Duhem integration is performed using two NPT simulations in parallel. Simulations were equilibrated for 20 million Monte Carlo steps and ran for 40 million Monte Carlo steps in production. Each NPT simulation was performed under the same conditions as described previously. The coexistence pressures were calculated using a simple predictor-corrector algorithm²³. With the predicted/corrected pressure, NPT simulations are done in parallel to obtain the next coexistence point, and the process is repeated until the full fluid-solid coexistence curve is obtained. This procedure was implemented for both systems at $\lambda = 1.15$ and $\lambda = 1.25$.

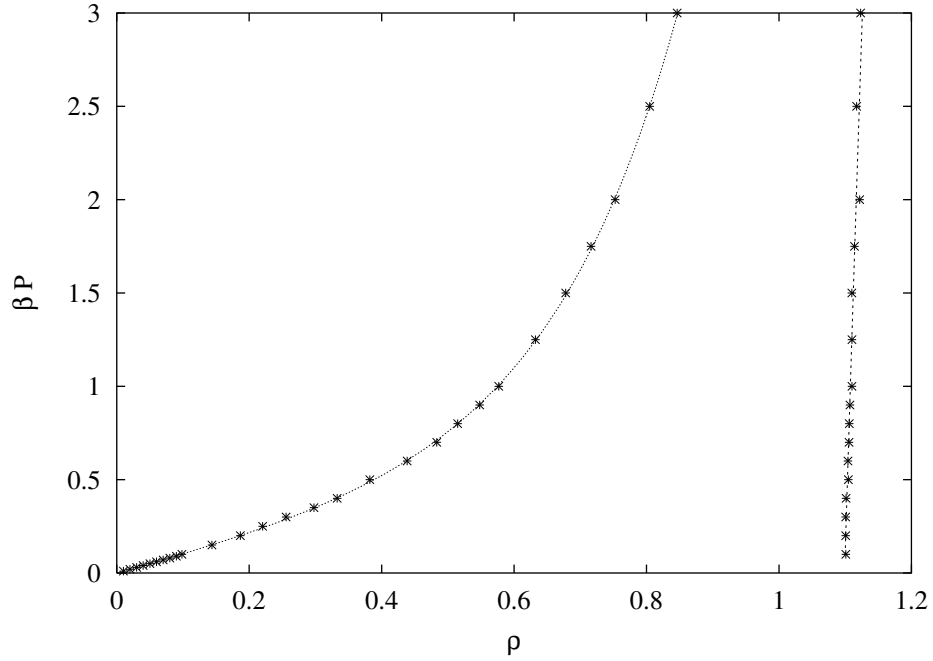


FIG. 2: Equation of state of the square well model for $\lambda = 1.15$. Also shown as the dashed lines are our fits according to equations in the text. Data was collected at the temperature $T = 1.0$.

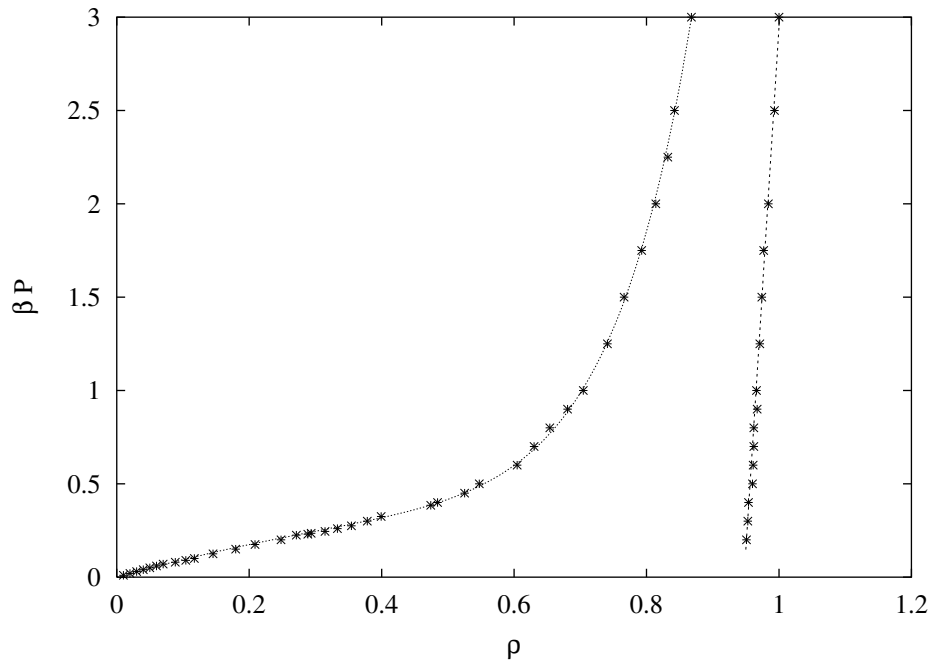


FIG. 3: Equation of state of the square well model for $\lambda = 1.25$. Also shown as the dashed lines are our fits according to equations in the text. Data was collected at the temperature $T = 1.0$.

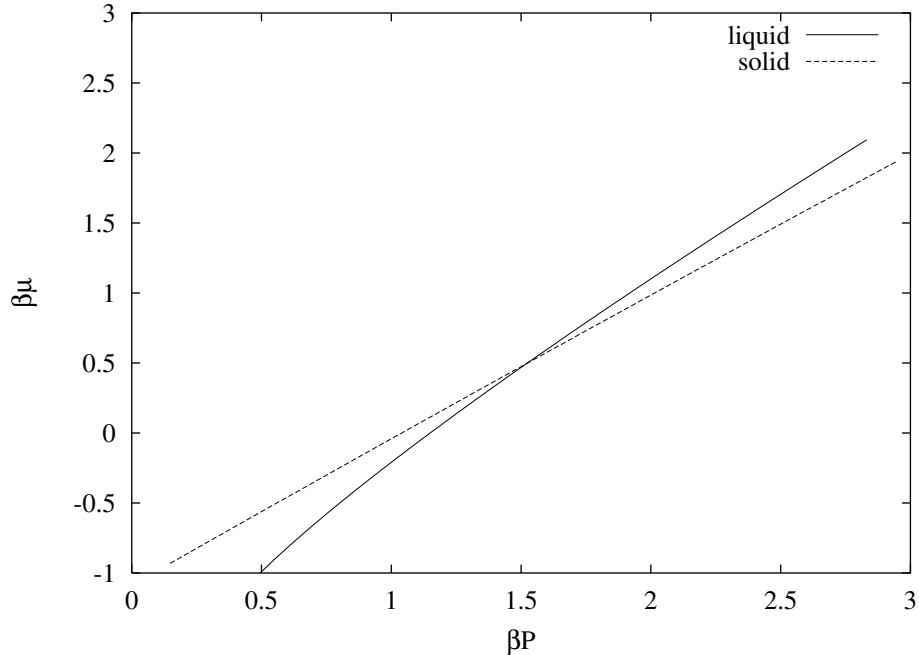


FIG. 4: Determination of a coexistence point for $\lambda = 1.25$. The point at which the curves cross satisfies the condition for coexistence, namely, equal chemical potentials at equal pressures.

B. Fluid-fluid coexistence

To calculate fluid-fluid coexistence of the square well model at $\lambda = 1.25$, we use the Gibbs ensemble Monte Carlo method²⁴. Two physically separated but thermodynamically connected simulation cells are used to calculate both the less dense and more dense fluid phases, respectively. This method circumvents the problem of an interface, which would hinder sampling, by altogether removing it. The two cells are allowed to exchange particles and both separately undergo volume displacements such that the total number of particles $N = N_1 + N_2$ and total volume $V = V_1 + V_2$ remain constant. Particles are also displaced within each cell according to the regular Metropolis method. Simulations for $N = 512$ particles were conducted on a periodic simulation cell. Simulations were equilibrated for 50 million steps and produced for 100 million steps. We required that the chemical potentials of both phases at each state point be equal to ensure coexistence had been reached.

At shorter interaction ranges, λ , it becomes increasingly difficult to sample phase space. The system becomes non-ergodic and standard techniques used to calculate fluid-fluid coexistence are unable to obtain coexistence points. As λ is decreased, the critical temperature T_c is decreased, and the particles tend to 'stick' together. Stickiness^{5,26} is a phenomenon

usually associated with the adhesive hard-sphere model²⁵. It is not unusual, therefore, that for sufficiently short-range square-well potentials stickiness begins to manifest itself. (An adhesive sphere interaction can be derived from a square-well interaction in the limit where the well becomes infinitesimally narrow and infinitesimally deep.)

To overcome this difficulty, we employ parallel-tempering²⁷ Monte Carlo to speed up equilibration of the system. Parallel tempering allows local Monte Carlo simulations (replicas) to communicate and exchange information between each other. The benefit of this is that systems that were unable to properly sample phase space are able to do so. Parallel tempering is quickly becoming a standard method of sampling systems that become trapped in local energy minima^{26,29,30}. We set up global Monte Carlo simulations using grand canonical Monte Carlo simulations in each replica, where each replica is allowed to exchange particle-configurations according to

$$p_{acc}(x_i \leftrightarrow x_{i+1}) = \min[1, \exp(-\Delta\mu\Delta N)], \quad (8)$$

where x_i is the state of the i^{th} replica and μ is the reduced chemical potential $\mu/k_B T$. The potential used is actually $\mu^* = \mu - 3 \ln[\Lambda/\sigma]$ (as in Ref²⁸). In what follows, we denote μ^* as μ for simplicity. To ensure detailed balance is obeyed, a replica is selected at random and tested to swap particle-configurations with a neighboring replica according to the above probability. Within each replica three trial moves are attempted: 1) insertion/deletion trial moves are attempted according to standard Monte Carlo as adapted for use in the grand canonical ensemble²⁸, 2) particle displacements are employed according to the regular Metropolis method, and 3) cluster moves³¹ are attempted to break-up any small clusters that may have formed. The last trial move is similar to those of particle displacements, however, extra care must be taken so that detailed balance is observed. Thus, a cluster of particles is displaced such that no new clusters are formed and no old clusters are destroyed.

Periodic boundary conditions are used for a simulation cell of size $L = 8\sigma$. Simulations were equilibrated for 10 million steps and production runs lasted 100 million steps. At each state point we chose to run our replicas at a common temperature with each differing in chemical potential μ . We used 6 to 7 replicas per global simulation, choosing the chemical potentials such that approximately 20% of particle exchanges were accepted. Once a density distribution was obtained in this way, coexistence points were determined using an equal-

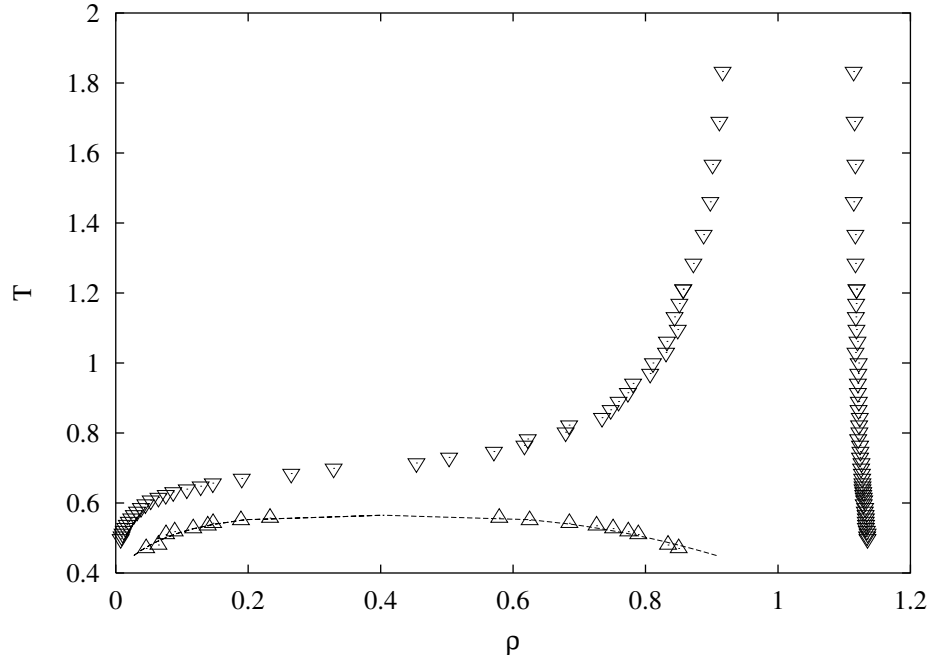


FIG. 5: Phase diagram of square well model for $\lambda = 1.15$ using Monte Carlo methods described in the text. Shown are the fluid-solid (∇) and metastable fluid-fluid (\triangle) coexistence curves along with our fit (solid line) to the latter.

area criterion according to

$$\int_0^{\langle \rho \rangle} P_L^{(\beta', \mu')}(\rho) = 0.5. \quad (9)$$

To facilitate our grand canonical simulations, we employ histogram-reweighting³² after each set of simulations. This method allows information at one state point to be obtained from a neighboring one, such that

$$P_L^{(\beta', \mu')}(\rho, u) = \frac{\exp[(\mu' - \mu)\rho V - (\beta' - \beta)uV] P_L^{(\beta, \mu)}(\rho, u)}{\sum \exp[(\mu' - \mu)\rho V - (\beta' - \beta)uV] P_L^{(\beta, \mu)}(\rho, u)}. \quad (10)$$

III. RESULTS AND DISCUSSION

We calculated the phase diagrams of the square well model for both $\lambda = 1.15$ and $\lambda = 1.25$, respectively. Our equations of state for both interaction ranges, simulated at the isotherm $T = 1.0$, are shown in Figs. 2 and 3. Our fits to the data are also shown in these figures,

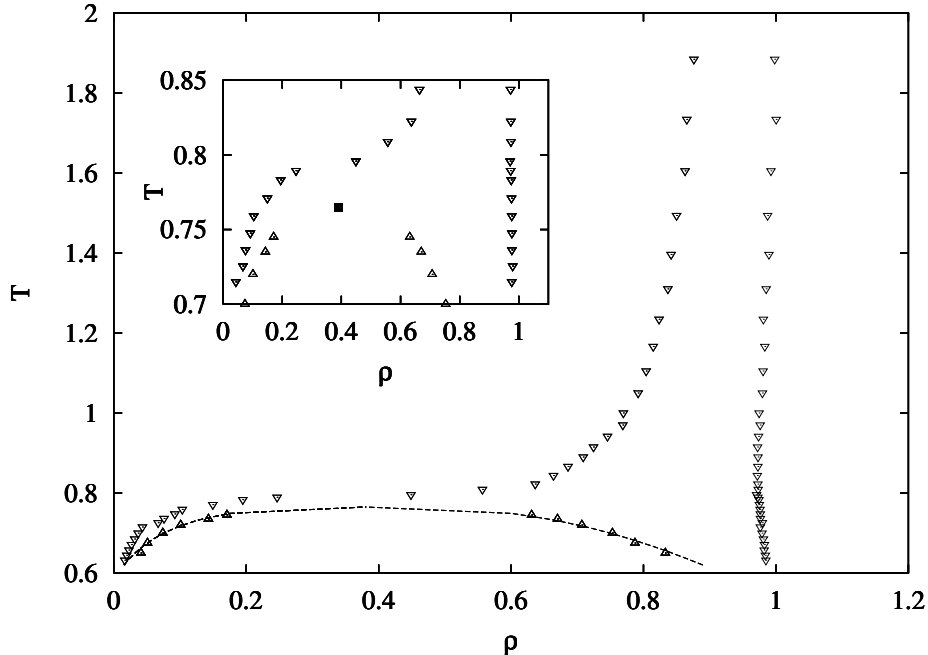


FIG. 6: Phase diagram of square well model for $\lambda = 1.25$ using Monte Carlo methods described in the text. Shown are the fluid-solid (∇) and metastable fluid-fluid (\triangle) coexistence curves along with our fit (solid line) to the latter. The inset shows a close-up view of the phase diagram near the estimated critical point (\blacksquare).

TABLE I: Results from fit to fluid-fluid coexistence curves

λ	T_c	ρ_c	ϕ_c	A	B
1.15	0.565(3)	0.404(3)	0.212	0.55(2)	0.89(1)
1.25	0.765(2)	0.390(4)	0.204	0.50(2)	0.82(1)

as described previously in the text. We emphasize the importance of obtaining very good fits to the data, as one must have accurate values of the chemical potentials of the two phases, vis-a-vis eqs. (4) and (5). Errors in fitting the data, particularly for the liquid, lead to errors in the value for a coexistence point and, ultimately, in determining the fluid-solid coexistence phase boundaries. Care was taken such that deviations between the data and the fit were usually less than 1.0%, no data point deviated from the fit by more than 3.0% for either model. Certain data points were obtained by running longer simulations to minimize fluctuations.

After obtaining good fits to our isotherms, we obtained coexistence points for the square

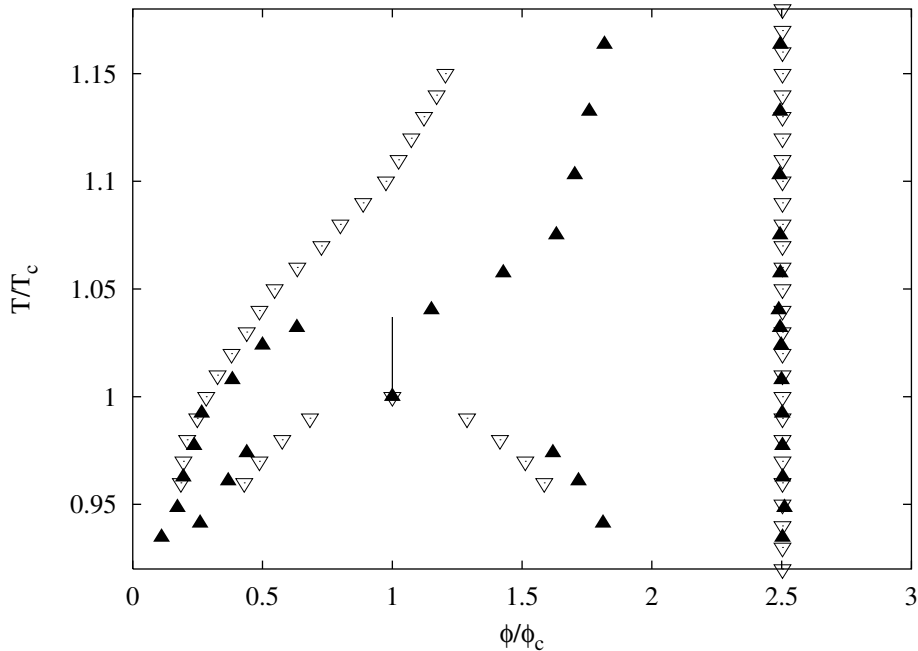


FIG. 7: Comparison of our Monte Carlo results (\blacktriangle) to the cell model results of Ref. ⁹ (∇) for the range $\lambda = 1.25$. Also plotted are our estimates of the critical temperature T/T_c . The metastability gap is represented as a solid line.

well models. This is shown in Fig. 4 where a coexistence point for $\lambda = 1.25$ has been determined by comparing the chemical potential versus pressure. We then employed the Gibbs-Duhem method for each model to obtain the fluid-solid coexistence curve. Figs. 5 and 6 show the phase diagrams for both interaction ranges studied. It can be seen that for $\lambda = 1.15$ the metastable fluid-fluid coexistence curve is far below the liquidus line. This curve clearly indicates that the threshold for metastability lies above this value for the interaction range. Other studies^{16,33,34} have been done on the Yukawa and square well models for extremely short range interactions. There, a phenomenon of isostructural solid-solid coexistence is observed, with the appearance of a solid-solid critical point. We observe no such coexistence at $\lambda = 1.15$, although we have not extended our simulations to high densities where such a phenomenon has been observed at lower ranges. Fig. 6 shows the phase diagram for $\lambda = 1.25$, showing that the fluid-fluid coexistence curve is metastable. We note that at the liquidus line just above the critical temperature, T_c , simulations exhibited large fluctuations in the density. We therefore ran longer simulations in this region than for other parts of the fluid-solid phase diagram to minimize fluctuations.

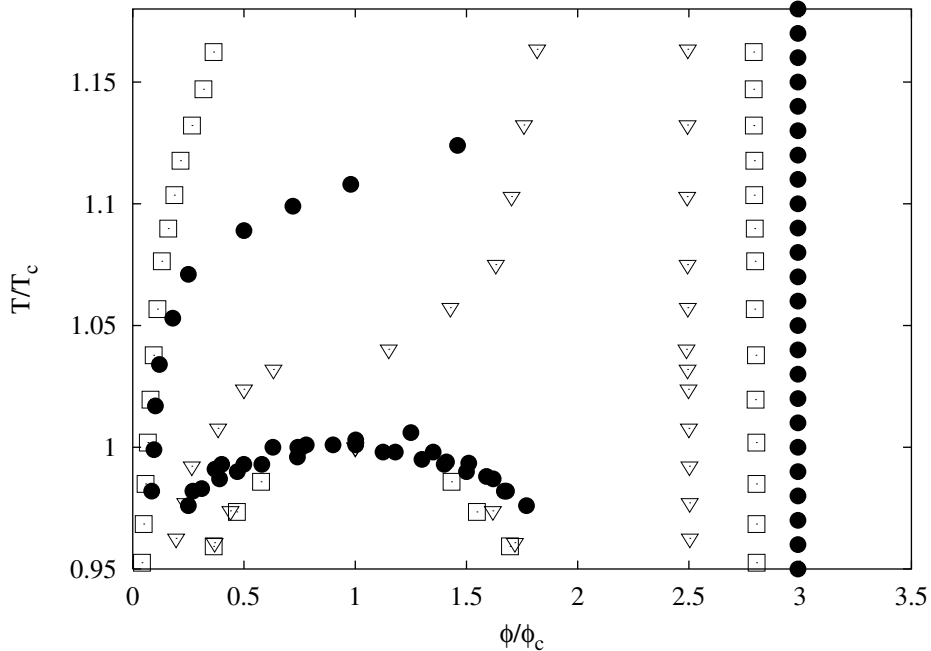


FIG. 8: Comparison of our Monte Carlo results for both $\lambda = 1.15$ (\square) and $\lambda = 1.25$ (∇), respectively, to the gamma-II crystallin (\bullet).

Also shown in Figs. 5 and 6 are our attempts to fit the metastable fluid-fluid coexistence curves to the equation $\rho_{\pm} - \rho_c = A|T - T_c| \pm B|T - T_c|^{\beta}$, where T_c and ρ_c are the critical temperature and density, respectively, and $\beta = 0.3258$ (Ref³⁵) is the Ising exponent. Table I shows our values for both $\lambda = 1.15$ and $\lambda = 1.25$. Our estimates compare well with other predictions^{9,11} of the critical point for these two ranges. The critical density ρ_c is shifted toward a higher density for $\lambda = 1.15$ as compared to that at $\lambda = 1.25$, as shown in Table I, but is smaller than the critical density predicted in (Ref^{9,41}).

As noted in the introduction, many models capture the qualitative characteristics of protein phase diagrams. It is interesting, however, that the Yukawa, MLJ, and 2n-n Lennard Jones models all have been shown¹⁰ to become metastable at the interaction range $R = \lambda - 1 = 0.13 - 0.15$. As noted, this is not, however, the case for the square well model. Our results confirm that $R \simeq 0.25$, as previous^{9,12} studies have predicted.

In another study⁹ of the square well model at $\lambda = 1.25$, the authors obtain the phase diagram by a combination of Monte Carlo and extrapolation techniques⁴¹. We compare our phase diagram at $\lambda = 1.25$ to theirs in Fig. 7, converting to the units T/T_c and volume fraction ϕ/ϕ_c (ρ/ρ_c). It is observed that both studies predict similar behavior for both the solidus line and metastable fluid-fluid coexistence curve. The liquidus lines, however, are

not compatible. We quantify this discrepancy by measuring the metastability gap, defined by⁹

$$\frac{T_L - T_c}{T_c} = \frac{n_s - n_s^*}{n_s^* - n_l} \quad (11)$$

where n_i are phenomenological values used in their model. Using this definition we find the gap values 0.240 for $\lambda = 1.15$ and .035 for $\lambda = 1.25$ for the metastability gaps. The former predictions⁹ overestimate the metastability gap by approximately 50% and 60%, respectively. The fact that our results for the solidus line agree with the early study is probably due to the fact that their choice for the number of contacts a given particle has within its interaction range in their cell model approximation is consistent with the fcc crystal structure for this model.

Much interest has been focused on the gamma crystallins³⁶, a group of monomeric eye lens proteins. Certain mutations³⁷ of these proteins has been linked to genetic cataracts and protein crystallization¹⁴. These proteins have been well studied¹³ and their phase behavior are similar to those of the square well model, warranting a comparison of the two. Fig. 8 shows our square well phase diagrams to those⁹ of the gamma-II crystallins. Although we compare our data with the gamma-II crystallin, it has been shown⁴¹ that the data for the fluid-fluid coexistence curve of the entire gamma crystallin family lies on the same curve, within the scatter of the data. Our values for ϕ_c , shown in Table I, are close to that of the value for the family of gamma crystallins. Both models qualitatively capture the characteristics of the gamma protein, with the model at the range $\lambda = 1.15$ more closely resembling it. The case $\lambda = 1.15$ yields better agreement with the liquidus and solidus lines than the model with $\lambda = 1.25$. For both models, however, the fluid-fluid coexistence curve is not as broad as that of the gamma-II crystallin. Indeed, some studies^{38,39} have attempted to remedy this by including anisotropy in the interactions among particles in the square well model, thereby broadening the fluid-fluid coexistence curves. One study³⁸ averages out the rotational degrees of freedom to obtain an effective temperature-dependent isotropic potential that better approximates both the liquidus and metastable fluid-fluid coexistence curves of the gamma-IIIb crystallin.

IV. CONCLUSION

The square well model for the interaction ranges $\lambda = 1.15$ and $\lambda = 1.25$ have been obtained using Monte Carlo simulations, including parallel tempering. We find that the latter interaction range is just below the threshold value for metastability of the fluid-fluid coexistence curve. Finite-size effects have not been taken into account for either the liquidus line or metastable fluid-fluid coexistence curve near the critical point where critical fluctuations could affect our results. However, the metastability gap is sufficiently large that we believe our conclusion about the metastable nature of the coexistence curve for $\lambda = 1.25$ is correct. We have also compared our Monte Carlo results for the complete phase diagram at $\lambda = 1.25$ to another study⁹ and find that this study does not predict the correct liquidus line. The complete phase diagram at $\lambda = 1.15$ was obtained by using standard Monte Carlo techniques, overcoming the problem of 'stickiness' by using parallel tempering for the fluid-fluid coexistence curve. A comparison of these two phase diagrams with the gamma-II crystallin has been made. Better qualitative agreement is obtained at $\lambda = 1.15$ with the experimental results for the gamma-II crystallin, but there is no quantitative agreement.

Isotropic fluids cannot be expected to quantitatively match experimental systems. Although certain characteristics of the phase diagrams of proteins can be captured by these simple models, it is unlikely that a correct solidus line can be obtained. This is due to anisotropic interactions and the (non spherical) ellipsoidal shape of certain globular proteins, such as the gamma crystallins⁴⁰. Models such as the square well model, or similar ones, alone, cannot account for effects such as anisotropy, solvent-solute interactions, or hydration effects commonly found in experimental systems and are, thus, too simple to be quantitatively accurate. However, the isotropic models do seem to provide a useful first approximation which can then be extended to include effects such as anisotropy and hydrophobicity.

V. ACKNOWLEDGEMENTS

This work is supported by NSF grant DMR0302598.

- ¹ A. P. Gast, C. K. Hall, and W. B. Russel, *J. Colloid Interface Sci.*, **96**, 251 (1983)
- ² H. N. W. Lekkerkerker *et al.*, *Europhys. Lett.*, **20**, 559 (1992); Tejero *et al.*, *Phys. Rev. Lett.*, **73**, 752 (1994)
- ³ S. M. Ilett *et al.*, *Phys. Rev. E*, **51**, 1344 (1995)
- ⁴ M. Muschol and F. Rosenberger, *J. Chem. Phys.*, **107**, 1953 (1997)
- ⁵ D. Rosenbaum, P.C. Zamora, and C.F. Zukoski, *Phys. Rev. Lett.*, **76**, 150 (1996)
- ⁶ M. H. J. Hagen and D. Frenkel, *J. Chem. Phys.* **101**, 4093, (1994)
- ⁷ P. R. ten Wolde and D. Frenkel, *Science* **277**, 1975 (1997)
- ⁸ D. W. Oxtoby and V. Talanquer, *J. Chem. Phys.* **101**, 223 (1998)
- ⁹ N. Asherie, A. Lomakin, and G. B. Benedek, *Phys. Rev. Lett.* **77**, 4832 (1996)
- ¹⁰ Massimo G. Noro and Daan Frenkel, *J. Chem. Phys.* **113**, 2941 (2000)
- ¹¹ L. Vega, E. de Miguel, L. F. Rull, G. Jackson and I. A. McLure, *J. Chem. Phys.***96**, 2296 (1992)
- ¹² A. Daanoun, C.F. Tejero, and M. Baus, *Phys. Rev. E* **50**, 2913 (1994); C. Rascón, G. Navasqués, and L. Mederos, *Phys. Rev. B* **51**, 14899 (1995)
- ¹³ M. L. Broide *et al.*, *Proc. Natl. Acad. Sci. USA* **88**, 5660 (1991); C. R. Berland *et al.*, *ibid*, **89**, 1214 (1992)
- ¹⁴ S. Kmoch *et al.*, *Human Molecular Genetics* **9**, 1779 (2000); A. Pande *et al.*, *Proc. Natl. Acad. Sci. USA* **98**, 6116 (2001)
- ¹⁵ N. M. Dixit and Charles F. Zukoski, *Journal of Colloid and Interface Science* **228**, 359 (2000)
- ¹⁶ G. Foffi *et al.*, *Phys. Rev. E* **65**, 031407 (2002)
- ¹⁷ D. A. Kofke, *J. Chem. Phys.* **98**, 4149 (1993); *ibid*, *Mol. Phys.* **78**, 1331 (1993)
- ¹⁸ We use different forms of the Clausius-Clapeyron equation at high and low temperatures to minimize numerical errors as in Refs. (^{6,17,19})
- ¹⁹ M. G. Noro and D. Frenkel, *J. Chem. Phys.* **114**, 2477 (2001)
- ²⁰ D. Frenkel and A.J.C. Ladd, *J. Chem. Phys.* **81**, 3188 (1984)
- ²¹ To correct for finite-size effects for crystals with a fixed center of mass, we calculate the free-

- energy contribution for discontinuous potentials as in the following reference: J. M. Polson *et al.*, J. Chem. Phys. **112**, 5339 (2000)
- ²² D. Frenkel and B. Smit, *Understanding Molecular Simulation*, (San Diego, Academic Press 2002)
- ²³ Numerical Recipes Online, World Wide Web, <http://www.library.cornell.edu/nr>
- ²⁴ A. Z. Panagiotopoulos, Mol. Phys. **61**, 813 (1987)
- ²⁵ R. J. Baxter, J. Chem. Phys. **49**, 2770 (1968)
- ²⁶ M. A. Miller and D. Frenkel, Phys. Rev. Lett. **90**, 135702, (2003)
- ²⁷ C. J. Geyer and E. A. Thompson, J. Am. Stat. Assoc. **90**, 909 (1995)
- ²⁸ M. P. Allen and D. J. Tildesley, *Computer Simulations of Liquids*, (Clarendon, Oxford, 1990)
- ²⁹ Q. Yan and J. J. de Pablo, J. Chem. Phys. **111**, 9509 (1999)
- ³⁰ D. L. Pagan, M. E. Gracheva, and J. D. Gunton, J. Chem. Phys. **120**, 8292 (2004)
- ³¹ N. A. Seaton and E. D. Glandt, J. Chem. Phys. **84**, 4595 (1986)
- ³² R. H. Swendsen, Physica A **194**, 53, (1993)
- ³³ P. and D. Frenkel, Phys. Rev. Lett. **72**, 2211 (1994)
- ³⁴ C. Rascón, L. Mederos, and G. Navascués, Phys. Rev. Lett. **77**, 2249 (1996); *ibid*, J. Chem. Phys. **103**, 9796 (1995)
- ³⁵ A. M. Ferrenberg and D. P. Landau, Phys. Rev. B **44**, 5081 (1991)
- ³⁶ J. Graw, Biol. Chem. **378**, 1331 (1997)
- ³⁷ D. A. Stephan *et al.*, Proc. Natl. Acad. Sci. USA **96**, 1008 (1999); A. Pande *et al.*, Proc. Natl. Acad. Sci. USA **97**, 1993 (2000)
- ³⁸ A. Lomakin, N. Asherie, and G. B. Benedek, Proc. Natl. Acad. Sci. USA, **96**, 9465 (1999)
- ³⁹ N. Kern and D. Frenkel, J. Chem. Phys. **118**, 9882 (2003)
- ⁴⁰ Ajit Basak *et al.*, J. Mol. Biol. **328**, 1137 (2003)
- ⁴¹ A. Lomakin, N. Asherie, and G. B. Benedek, J. Chem. Phys. **104**, 1646 (1996)